

MEMORANDUM

Anchorage

DATE: January 25, 2001

TO: Embankment Technical Review Board
Attn: Pete Douglass

Boston

FROM: Douglas Lindquist, EIT, Michael Bailey, P.E., Hart Crowser, Inc.

RE: **Additional Information on the Seismic Design**
J-4978-30

Chicago

CC: Jim Thomson, P.E., HNTB

Denver

This memorandum provides additional information regarding the seismic analyses performed for the Third Runway at the Sea-Tac International Airport in SeaTac, Washington. This discussion includes the probabilistic seismic hazard analysis (PSHA) and the ensuing ground response analyses used to provide the basis for analysis of seismic stability, deformation, and liquefaction potential. This memorandum provides an overview and details for the following:

Portland

1. Seismic Sources;
2. Attenuation Relationships;
3. Results of the PSHA;
4. Input Motion Development; and
5. One-Dimensional Site Response Analysis.

Seattle

San Francisco

San Jose

OVERVIEW OF PROBABILISTIC SEISMIC HAZARD ANALYSIS

San Diego

Seismically induced ground motions at the Third Runway site can be produced by earthquakes from a number of different shallow and deep sources spread throughout the greater Puget Sound region. Hart Crowser and subconsultant Professor Steven L. Kramer

Seattle



used a probabilistic seismic hazard analysis (PSHA) to evaluate ground motion characteristics for different seismic hazard levels. The characteristics of ground motions with different exceedence probabilities were evaluated by quantifying the uncertainties in earthquake magnitude, recurrence, and location, and by considering the uncertainties in ground motion parameter predictions.

The results of the PSHA indicate the probability that a certain level of ground shaking will be exceeded in any given time period, such as a seismic event with a 10 percent probability of exceedence in 50 years (475-year return period). Hart Crowser used the results of the PSHA and the site response analysis for different design tasks, including comparison of the risk of soil liquefaction for different seismic events and to provide input for stability and deformation analyses.

SEISMIC SOURCES

Seismic records in the Puget Sound area clearly indicate the existence of distinct shallow and deep zones of seismicity. As illustrated on Figure 1, the shallow crustal sources extend to depths of 25 to 30 km. The deeper zone is clearly associated with the subducting Juan de Fuca plate and produces earthquakes at depths of 45 to 70 km beneath the Puget Sound region and at shallower depths farther to the west. For seismic hazard analysis the shallow and deep zones are treated separately.

Shallow, Areal Sources

The shallow seismicity illustrated on Figure 1 was interpreted as having been produced primarily by any of a number of regional faults, many of which were not identified until after a seismic event. The area surrounding the Third Runway site was broken into six regional sources defined by the main physiotectionic provinces. These shallow regional sources consist of the Puget Sound Basin, Olympic Mountains, Willapa Hills, Southern Cascades, Northern Cascades, and Vancouver Island physiotectionic zones. The geometries of these zones are shown on Figure 2.

The Gutenberg-Richter Recurrence Law was used to obtain recurrence relationships for the regional sources. This recurrence law may be expressed as:

$$\log \lambda_m = a - b M_w$$



where:

λ_m is the annual rate of exceedence of magnitude, M_w ,

10^a is the yearly number of earthquakes greater than the minimum value (in this analysis, $M_{w(\min)} = 2$), and

b is a constant that reflects the relative likelihood of large versus small earthquakes. A high b value indicates a source that produces relatively few large earthquakes relative to the number of small earthquakes.

The recurrence relationships were obtained from a database of seismic events of magnitude greater than 2.0 occurring between latitudes 45°N and 49°N and between longitudes 120°W and 125°W during the period between December 2, 1841, and August 31, 1999 (Kramer, 1999). To produce recurrence data, the following steps were used to process the database:

1. The raw database, which included reports from several networks of recording stations, contained over 10,000 entries. In a number of cases, a single seismic event was recorded by multiple stations and, consequently, was described by more than one entry in the database. To avoid counting the same event more than once, the database was searched to remove multiple entries. This process removed approximately 40 percent of the entries from the database.
2. The raw database included all recorded events of magnitude greater than 2.0 in the spatial and temporal window described above. The raw database made no distinction between independent events and dependent events such as aftershocks and foreshocks. A modified version of the procedure of Gardner and Knopoff (1974), which assigned aftershock weighting factors based on spatial and temporal proximity to a main shock, was applied to the entire database to identify dependent events. Events with aftershock weighting factors greater than 0.95 were removed from the database. The remaining events were assigned event weighting factors equal to $1-w$ where w was the aftershock weighting factor. The event weighting factor was equal to 1.0 for most of the remaining events.
3. The database was parsed on a magnitude-dependent basis using the completeness intervals of Ludwin et al. (1991) to ensure appropriate recurrence rates.

AR 049836

STIA 00521



4. The corrected database was divided into shallow and deep events accounting for the sloping nature of the Cascadia Subduction Zone.
5. The remaining shallow database was divided into six individual databases consisting of events with epicenters within the six areas source zones listed previously.
6. Area-normalized recurrence relationships were determined individually for each of the six sources. The area-normalized recurrence relationships for the shallow sources were then multiplied by the area of each source. The resulting relationships, summarized below, were used in the PSHA.

Puget Sound Basin	$\log \lambda_m = 2.861 - 0.801 M_w$
Olympic Mountains	$\log \lambda_m = 1.628 - 0.619 M_w$
Willapa Hills	$\log \lambda_m = 1.771 - 0.800 M_w$
Southern Cascades	$\log \lambda_m = 3.139 - 0.795 M_w$
Northern Cascades	$\log \lambda_m = 2.383 - 0.725 M_w$
Vancouver Island	$\log \lambda_m = 1.623 - 0.633 M_w$

Seattle Fault

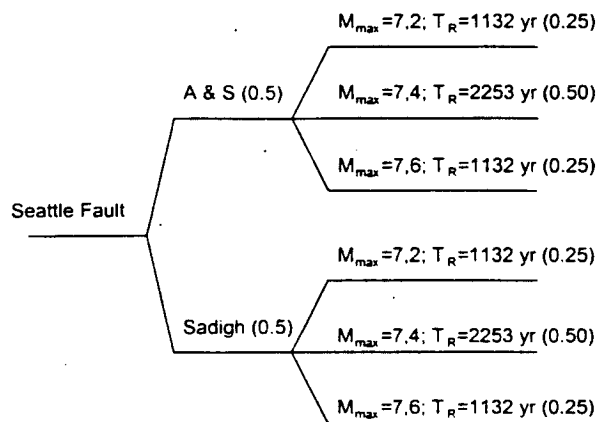
The Seattle Fault has been extensively investigated in recent years and knowledge of its structure and recurrence behavior has improved. Pratt et al. (1997) developed the most recent model of the Seattle Fault; the geometry and mechanisms of this model are consistent with estimated slip and recurrence rates, and with available paleoseismological data. This model forms the basis for the characterization of the Seattle Fault employed in this hazard analysis.

The Seattle Fault is a south-dipping thrust fault that runs in a generally east-west direction from the Kitsap Peninsula to the Cascade foothills. Its maximum rupture length is estimated to be about 65 km. The fault dips at an angle of approximately 20 degrees, but steepens to an angle of about 45 degrees within the upper 3 to 4 km (Pratt et al., 1997). The downdip extent coincides with a lineament at the north edge of the Tacoma basin that has been mapped as the "Tacoma Fault" (Gower et al., 1985; Rogers et al., 1996). This boundary produces a downdip width of 32 to 43 km.

The dimensions of the fault suggest that the maximum magnitude for the Seattle Fault has a mean value of approximately 7.4 with a standard deviation of about 0.2. As a result, the maximum magnitude was characterized using the following magnitudes (and weighting factors): 7.2 (0.25), 7.4 (0.50), and 7.6 (0.25).



Seattle Fault slip rates have been estimated at 0.07 to 0.11 cm/yr from offsets observed during recent geophysical investigations (Johnson et al., 1999). Using the best estimate of the fault area and the maximum magnitude, such slip rates would be consistent with mean recurrence intervals of 1,132, 2,253, and 4,506 years for earthquakes of magnitude 7.2, 7.4, and 7.6, respectively. These recurrence intervals are consistent with the reported results of recent fault trenching studies on Bainbridge Island, which suggest that three to four events have ruptured the ground surface of the Toe Jam Hill strand of the Seattle Fault in the past 12,000 years. Weighted values of relative magnitude and recurrence interval for different estimates of the Seattle Fault are illustrated below.



Cascadia Subduction Zone

The Cascadia Subduction Zone (CSZ) lies off and below the coast of Washington where the Juan de Fuca plate plunges beneath the North American plate. Two types of earthquakes are associated with the CSZ—intraplate and interplate events. Because the two types of events involve different mechanisms on different parts of the CSZ, they are considered to be independent of each other and are considered in this hazard analysis to be two separate sources.

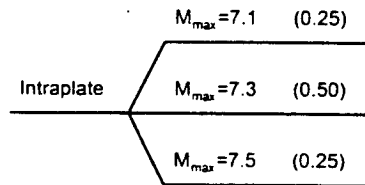
Intraplate Events

CSZ intraplate events are associated with extension (normal faulting) events in the upper portion of the Juan de Fuca plate where its inclination becomes steeper beneath the Puget Sound basin. The existence of intraplate earthquakes has been well established for many years. The 1949 Olympia (M7.1) and 1965 Seattle-Tacoma (M6.5) earthquakes are



examples of CSZ intraplate events. Nearly all CSZ intraplate events detected by modern instrumentation have occurred at focal depths of 30 to 75 km. This portion of the CSZ was modeled with a series of 19 trapezoidal planar elements whose shapes approximated the contours on Figure 4 at depths of approximately 30 to 75 km.

Intraplate earthquakes such as those that occur on the CSZ involve high-angle normal faulting; as a result, the available fault rupture area is constrained by the thickness of the subducting plate. In other parts of the world, intraplate earthquakes of up to M7.5 have been observed; the largest of these have occurred in relatively old and thick subducting plates. The relatively young age of the CSZ indicates that the thickness of the Juan de Fuca plate should be low; thermal modeling studies (e.g., Hyndman and Wang, 1993 and 1995) and the observed geometry of the CSZ Benioff zone (Jarrard, 1986) are consistent with a thin subducting plate. These conditions suggest that the maximum magnitude of CSZ intraplate earthquakes could range from 7.1 to 7.5; values of 7.1 (0.25), 7.3 (0.50), and 7.5 (0.25) were used in this hazard analysis. Weighted values of relative magnitude and recurrence interval for different estimates of the CSZ intraplate events are illustrated below.



The recurrence relationship for CSZ intraplate events was based on historical seismicity and modeled using a truncated Gutenberg-Richter recurrence relationship. The Gutenberg-Richter relationship had values of $a = 2.219$ and $b = 0.652$.

Interplate Events

CSZ interplate events occur when rupture occurs by a shearing (reverse faulting) mechanism on the locked portion of the subduction zone. Paleoseismological evidence (Atwater, 1987 and 1992; Atwater and Hemphill-Haley, 1997) indicates that seven distinct interplate events have occurred on the CSZ within the past 3,500 years.

While the geometry of the CSZ is relatively well known from measured hypocentral locations (Crosson and Owens, 1987), the geometry of the seismogenic (locked) portion is less well established. The seismogenic portion is bounded in both the updip and downdip directions. At shallow depths, weak accretionary sediments and potentially high pore pressures allow ductile (aseismic) plate motion to occur; these conditions control the updip



boundary of the seismogenic zone. At large depths, temperatures become high enough that the rock behaves in a ductile (aseismic) manner; these depths control the downdip boundary of the seismogenic zone.

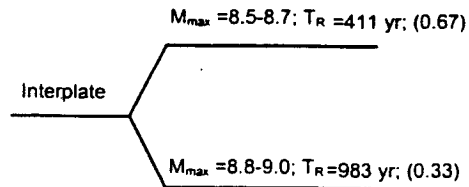
Two updip boundary locations have been proposed. Hyndman and Wang (1993) suggested that the clays that exist within the CSZ would be sufficiently dehydrated at temperatures above 100°C to 150°C to produce brittle behavior, and thermal modeling indicated that such temperatures would be reached near the deformation front. Mapping of folds and faults in north-central Oregon has identified a slope break approximately 30 km east of the deformation front, which has also been postulated as representing the updip boundary of the CSZ (Goldfinger et al., 1992).

Two downdip boundary locations have also been reported in the literature. Distortion of the overriding plate has produced a consistent pattern of uplift and subsidence in other subduction zones around the world. The point that separates regions of uplift and subsidence, termed the "zero isobase," has been shown to coincide with the downdip extent of rupture in past interplate earthquakes and was used as a downdip boundary in this PSHA. The downdip boundary can also be located using thermo-mechanical considerations. Silicic rock typically exhibits ductile behavior at temperatures above 350°C to 450°C (Tichelaar and Ruff, 1993). Hyndman and Wang (1993) modeled the thermal environment along the CSZ to determine the depths at which various temperatures occurred. Using the 350°C contour as representing the downdip boundary of the fully locked zone and the 450°C contour as the updip boundary of the fully uncoupled zone, the mid-point of the "transition zone" (the zone where temperatures are between 350°C and 450°C) can provide a reasonable estimate of the downdip boundary. For the purposes of this hazard evaluation, the two postulated updip boundaries and two postulated downdip boundaries were weighted equally to determine the average width of the seismogenic portion of the CSZ. This average width was 70 km.

Considering the 1,100 km length of the CSZ and the average 70 km width, empirical correlations indicate a mean maximum magnitude of 8.7 with a standard deviation 0.3. While no interplate earthquakes have been instrumentally recorded, other techniques have been used to identify their past occurrence. Atwater and Hemphill-Haley (1997) recently completed a detailed investigation of CSZ interplate earthquake recurrence intervals using geologic, turbidite, and buried soil evidence. The geologic evidence suggests a recurrence interval distribution with a mean value of 660 years, a standard deviation of 200 years, and a coefficient of skewness of 1.06. The turbidite evidence suggests corresponding values of 620 years, 290 years, and 0.80; and the buried soil evidence suggests values of 520 years, 301 years, and 0.29. Weighting these three forms of evidence equally, the mean recurrence



interval is 600 years with a standard deviation of 270 years and a coefficient of skewness of 0.72. Using a point estimation technique to match the mean, standard deviation, and coefficient of skewness of the estimated recurrence interval distribution, the CSZ interplate event was modeled using two alternative scenarios—a characteristic earthquake of M8.5 to M8.7 with a return period of 411 yrs and a characteristic earthquake of M8.8 to M9.0 with a return period of 983 yrs. The weighting factors for the two scenarios were 0.67 and 0.33, respectively. Weighted values of relative magnitude and recurrence interval for different estimates of the CSZ interplate events are illustrated below.



Puget Sound Fault

Recent seismic reflection profiling in Puget Sound identified a 55-km-long, north-south trending zone of nearly vertical strike-slip fault strands, which is referred to as the Puget Sound Fault (Johnson et al., 1999). The depth of the Puget Sound Fault has not been determined, but is at least 6 km (Johnson et al., 1999) and more likely on the order of 15 to 20 km. Using the empirical correlation of Wells and Coppersmith (1994), the mean maximum magnitude is estimated at approximately M7.1 with a standard deviation of 0.28. For this hazard analysis, a characteristic earthquake recurrence model with characteristic earthquakes ranging from M6.8 to M7.4 was used.

Seismic refraction data suggest slip rates of 0.03 to 0.08 cm/yr for the Puget Sound Fault. For the mean maximum magnitude, the range of slip rates corresponds to recurrence intervals of 2,500 to 6,800 years. The mean value of 4,650 years was used for the Puget Sound Fault characteristic earthquake recurrence interval in this hazard analysis.

ATTENUATION RELATIONSHIPS

Three attenuation relationships were used in these analyses. Two equally weighted attenuation relationships were used for the shallow sources and one relationship was used for the two deep sources.



The Abrahamson and Silva (1997) attenuation relationship was used for the Puget Sound Basin, Olympic Mountains, Willapa Hills, Southern Cascades, Northern Cascades, Seattle Fault, and Puget Sound Fault source zones with a 50 percent logic tree weighting. In this analysis, reverse faulting and the hanging wall option were selected for the Seattle Fault source zone. The other sources were not modeled as reverse faults and did not have the hanging wall effect. The attenuation was used to compute ground motion parameters for a rock site.

The Sadigh et al. (1997) attenuation relationship was also used for the Puget Sound Basin, Olympic Mountains, Willapa Hills, Southern Cascades, Northern Cascades, Seattle Fault, and Puget Sound Fault source zones with a 50 percent logic tree weighting. In this analysis, reverse/thrust faulting was only selected for the Seattle Fault source zone, and the attenuation was run for a rock site.

The Youngs et al. (1997) attenuation relationship was used for the Cascadia Intraplate and Interplate source zones. In this analysis, the intraslab event type was used for the CSZ Intraplate source, and the interface event type was used for the CSZ Interplate source. Focal depths of 15 and 50 km were used for the interplate and intraplate sources, respectively. The attenuation was run for a rock site.

RESULTS OF THE PSHA

Peak Horizontal Acceleration

Overall seismic hazard for the Third Runway site is based on the summation of the seismic hazard by each seismic source. Figure 3 presents the total seismic hazard curve for peak acceleration as well as the seismic hazard curves for the individual source zones. The mean annual rate of return was used to compute probabilities of exceedence using the Poisson relationship, $p = 1 - e^{-\lambda}$. The peak acceleration corresponding to some often used exceedence probabilities are listed in Table 1.



Table 1 – Peak Horizontal Acceleration for Different Levels of Risk

Probability of Exceedence in 50 Years	Return Period in Years	Peak Horizontal Acceleration in g
50%	72	0.13
10%	475	0.35
5%	975	0.48
2%	2475	0.70

Spectral Acceleration

In addition to analysis of the peak horizontal acceleration, seismic hazard curves for spectral accelerations were calculated. These curves were used to determine spectral accelerations with various mean annual rates of exceedence. Figure 4 shows the site uniform risk spectra for four different return periods. The 475-year spectrum was used as input for developing seismic input motions.

Deaggregated Hazard

Deaggregation plots show the influence of magnitude and source-to-site distance on the seismic hazard at the Third Runway site. Three-dimensional plots of the deaggregated seismic hazard for the 475-year seismic event are presented on Figures 5, 6, and 7 for peak horizontal acceleration (PHA), a period of one half second, and a period of one second, respectively.

INPUT MOTION DEVELOPMENT

A set of spectrum-compatible ground motions were developed using the uniform hazard spectra developed in the PSHA. These motions were then propagated through soil profiles representing the site-specific conditions at the Third Runway site.

The uniform hazard spectra developed in the PSHA are representative of soft rock outcrop conditions. Deaggregation analyses were used to identify the magnitude and distance that contributed most strongly to the hazard at the site for each return period. These parameters were used to ensure that the spectrum-compatible motions had appropriate strong motion durations.



The ground motions were developed using the computer program, RASCAL (Silva, 1987). RASCAL uses a Brune spectrum and a seed motion to develop a ground motion that is compatible with a user-specified target spectrum. The uniform hazard spectra from the PSHA were used as the target spectra, and the parameters from the deaggregation analysis were used to develop the Brune spectra. RASCAL scales the Brune spectrum iteratively until it produces a spectrum-compatible ground motion when combined with the phase spectrum of the seed motion. The resulting motion has an amplitude and frequency content that is consistent with the results of the PSHA and a duration that is consistent with the results of the deaggregation analysis.

Selection of seed motions was accomplished carefully. A search of web-based ground motion databases was used to identify recorded ground motions with magnitudes, distances, and peak accelerations approximately equal to the values obtained from the PSHA/deaggregation analyses. Twenty-six candidate motions were identified. These motions were then scaled so that the average of their spectral accelerations at $T = 0.3$ and $T = 1.0$ sec were equal to the average values of those spectral accelerations from the uniform hazard spectra. The bracketed durations (0.05 g threshold acceleration) of the scaled motions were then computed. The scaled motions with bracketed durations closest to, but less than, the expected (soil) bracketed durations (Chang and Krinitszky, 1977) were selected for further evaluation. This process yielded three to five candidate motions for each return period. The Husid plots for each of these motions was examined for consistency with the shapes of Husid plots for typical earthquake ground motions; the two motions with the most appropriate Husid plots were subjectively identified and selected for use as seed motions. To reflect the importance of the Seattle Fault contribution to the hazard in the cases of the 975- and 2,475-year return periods, one of the two ground motions was required to use a near-fault motion as the seed motion for those cases. The seed motion time histories that were used to obtain the time histories used in the analyses are presented on Figure 8.

After confirming that the response spectra of the RASCAL motions were consistent with the uniform hazard spectra, the motions were baseline-corrected and converted to ProShake format for subsequent site response analysis.

The acceleration, velocity, and displacement time histories for the two motions developed for the 475-year return period are shown on Figures 9 and 10. The response spectra for 5 percent damping are shown on Figure 11. Figure 12 presents the Husid plots of acceleration for both motions. The Fourier amplitude spectra are shown on Figure 13.



ONE-DIMENSIONAL SITE RESPONSE ANALYSIS

One-dimensional site response analyses were performed to compute the ground motion characteristics at different elevations. The modulus reduction and damping curves used for the site soils and fill materials are shown on Figure 14.

The shear wave velocity at each wall was measured from down-hole testing. Because of their similarities, the velocity profiles were averaged into a single profile appropriate for the site. The shear wave velocity of the fill was predicted to be near 1,000 feet per second based on a N_{60} blow count of 50 blows per foot and a unit weight of 140 pounds per cubic foot (Imai and Tonouchi, 1982).

The site conditions were modified to account for the effect of compaction or consolidation of near-surface soils under the weight of the embankment. For the site response analyses, this was accomplished by changing the shear wave velocities (and the maximum shear modulus, G_{max}) to reflect the higher effective confining pressures that will exist after placement of the fill. The velocities were adjusted using the Ohta and Goto (1976) empirical relationship between G_{max} and $(N_1)_{60}$. The existing G_{max} and density values, (along with the water table depth) were used to backcalculate an "apparent" $(N_1)_{60}$ value for each layer. The increased mean effective stress that would exist in each layer after placement of the proposed embankment fill was calculated. New G_{max} values were then calculated using the apparent $(N_1)_{60}$ values and the new effective stresses. In this way, G_{max} values were consistent with the measured (pre-fill placement) values and also consistent with Ohta and Goto (1976). This procedure implicitly assumes that $(N_1)_{60}$ remains constant, or that increase in density will essentially be due to one-dimensional compression, so any increase in N-value due to the increased effective stress would be compensated for by the revised overburden correction.

An elastic compression approach was used to adjust density of the *in situ* soil resulting from the weight of the embankment. To obtain a Young's modulus for estimation of elastic compression, the shear wave velocity was used to calculate shear modulus and Poisson's ratio was assumed to be 0.3. Changes in density were insignificant and were thus neglected.



Figure 15 illustrates the shear wave velocity profiles that were used in the site response analysis. The "Existing Condition" profile represents the conditions prior to fill placement and the other two profiles were based on the updated shear wave velocities due to fill placement. The input motions created with RASCAL were applied at the base of the soil profile (250-foot depth) for the site response analyses. Ground motions were calculated for both the 50- and 150-foot fill conditions. Tables 2 and 3 show the peak horizontal acceleration for the top of fill, original ground surface, and approximate base of the FLAC model (37 feet below the current ground surface) for the 50- and 150-foot fill conditions, respectively.

Table 2 – 50-Foot Fill Condition: Peak Horizontal Acceleration at Different Depths

Depth	Peak Ground Acceleration	
	Input Motion A	Input Motion B
Top of Fill	0.34 g	0.32 g
Original Ground Surface	0.31 g	0.22 g
Base of FLAC (37.5 ft depth)	0.27 g	0.30 g



Table 3 – 150-Foot Fill Condition: Peak Horizontal Acceleration at Different Depths

Depth	Peak Ground Acceleration	
	Input Motion A	Input Motion B
Top of Fill	0.26 g	0.31 g
Original Ground Surface	0.26 g	0.29 g
Base of FLAC (37.5 ft depth)	0.23 g	0.24 g

F:\docs\jobs\497830\psha memo.doc

Attachments:

References

- Figure 1 - Typical Cross Section through Northwest Washington State
- Figure 2 - Shallow Seismic Source Zones Used in Recurrence Relationships
- Figure 3 - Seismic Hazard Curves for Peak Acceleration
- Figure 4 - Uniform Risk Spectra
- Figure 5 - Deaggregated Seismic Hazard, PHA, 475-yr seismic event
- Figure 6 - Deaggregated Seismic Hazard, T=0.5 second, 475-yr seismic event
- Figure 7 - Deaggregated Seismic Hazard, T=1.0 second, 475-yr seismic event
- Figure 8 - Time Histories of Acceleration - Seed Motions
- Figure 9 - Time Histories for Motion A
- Figure 10 - Time Histories for Motion B
- Figure 11 - Response Spectrum - 5 Percent Damping
- Figure 12 - Husid Plots of Input Motions
- Figure 13 - Fourier Amplitude of Acceleration
- Figure 14 - Modulus Reduction Curve and Damping Curve
- Figure 15 - Shear Wave Velocity Profiles

STIA 00532

AR 049847

REFERENCES

- Abrahamson, N.A. and W.J. Silva, 1997. "Empirical Response Spectral Attenuation Relations for Shallow Crustal Earthquakes," *Seismological Research Letters*, Vol. 68, No. 1, pp. 94-127.
- Atwater, B.F. and A.L. Moore, 1992. "A tsunami about 1000 years ago in Puget Sound, Washington," *Science*, Vol. 258, pp. 1614-1617.
- Atwater, B.F., 1992. "Geologic evidence for earthquakes during the past 2000 years along the Copalis River, southern coastal Washington," *Journal of Geophysical Research*, Vol. 97, pp. 1901-1919.
- Atwater, B.R. and E. Hemphill-Haley, 1997. "Recurrence intervals for great earthquakes of the past 3500 years at northeastern Willapa Bay, Washington," USGS Professional Paper 1576.
- Bucknam, R.C., E. Hemphill-Haley, and E.B. Leopold, 1992. "Abrupt uplift within the past 1700 years at southern Puget Sound, Washington," *Science*, Vol. 258, pp. 1611-1614.
- Chang, F.K. and E.L. Krinitsky, 1977. "Duration, spectral content, and predominant period of strong motion earthquake records from western United States," Miscellaneous Paper 5-73-1, U.S. Army Corps of Engineers, Waterways Experiment Station, Vicksburg, Mississippi.
- Crosson, R.S. and T.J. Owens, 1987. "Slab geometry of the Cascadia Subduction Zone beneath Washington from earthquake hypocenters and teleseismic converted waves," *Geophysical Research Letters*, Vol. 14, pp. 824-82.
- Gardner, J.K. and L. Knopoff, 1974. "Is the Sequence of Earthquakes in Southern California with Aftershocks Removed, Poissonian?," *Bulletin of the Seismological Society of America*, Vol. 64, No. 5, pp. 1363-1367.
- Geomatrix Consultants, 1995. "Final Report: Seismic Design Mapping, State of Oregon."
- Goldfinger C., L.D. Kulm, R.S. Yeats, C. Mitchell, R.E. Weldon III, C. Peterson, M. Darienzo, W. Grant, and G. Priest, 1992. "Neotectonic map of the Oregon continental margin and adjacent abyssal plain," Oregon Department of Geology and Mineral Industries Open-File Report 0-92-4, 17 pp.

Gower, H.D., J.D. Yount, and R.S. Crosson, 1985. "Seismotectonic Map for the Puget Sound Region, Washington," U.S. Geological Survey Miscellaneous Investigations Series Map I-1613, scale 1:250,000.

Hyndman R.D. and K. Wang, 1993. "Thermal constraints on the zone of major thrust earthquake failure: the Cascadia Subduction Zone," *Journal of Geophysical Research*, Vol. 98, pp. 2039-2060.

Hyndman, R.D. and K. Wang, 1995. "The Rupture Zone of Cascadia Great Earthquakes from Current Deformation and the Thermal Regime," *Journal of Geophysical Research*, Vol. 100, No. 22, pp. 133-154.

Imai, T. and K. Tonouchi, 1982. "Correlation of N-value with s-wave velocity and shear modulus," *Proceedings, 2nd European Symposium on Penetration Testing*, Amsterdam, pp. 57-72.

Jacoby, G.C., P.L. Williams, and B.M. Buckley, 1992. "Tree ring correlation between prehistoric landslides and abrupt tectonic events in Seattle, Washington," *Science*, Vol. 258, pp. 1621-1623.

Jarrard, R.D., 1986. "Relations among subduction parameters," *Review of Geophysics*, Vol. 24, No. 2, pp. 217-284.

Johnson, S.Y., S.V. Dadisman, J.R. Childs, and W.D. Stanley, 1999. "Active tectonics of the Seattle Fault and central Puget Sound, Washington - Implications for earthquake hazards," *Geological Society of America Bulletin*, Vol. 111, No. 7, pp. 1042-1053.

Karlin, R.E. and S.E.B. Abella, 1992. "Paleoearthquakes in the Puget Sound region recorded in sediments from Lake Washington, U.S.A.," *Science*, Vol. 258, pp. 1617-1620.

Kramer, S.L., 1999. Personnel communication.

Ludwin, R.S., C.S. Weaver, and R.S. Crosson, 1991. "Seismicity of Washington and Oregon," Slemmons, D.B., Engdahl, E.R., Zoback, M.D., and Blackwell, D.L., eds., *Nanotectonics of North America, Decade Map Volume 1*, Geological Society of America, Boulder, Colorado, pp. 77-98.

Ohta, Y. and N. Goto, 1976. "Estimation of s-wave velocity in terms of characteristic indices of soil," *Butsuri-Tanku*, Vol. 29, No. 4, pp. 34-41.

Pratt, T.L., S.Y. Johnson, C.J. Potter, et al. 1997. "Seismic reflection images beneath Puget Sound, Western Washington state," *Journal of Geophysical Research*, Vol. 102, pp. 469-490.

Rogers, A.M., T.J. Walsh, W.J. Kockelman, and G.R. Priest, 1996. "Earthquake hazards in the Pacific Northwest - An overview," in A.M. Rogers, T.J. Walsh, W.J. Kockelman and G.R. Priest (eds.), *Assessing Earthquake Hazards and Reducing Risk in the Pacific Northwest*, U.S. Geological Survey Professional Paper 1560, Vol. 1, pp. 1-54.

Sadigh, K., C.Y. Chang, J.A. Egan, F. Makdisi, and R.R. Youngs, 1997. "Attenuation relationships for shallow crustal earthquakes based on California strong motion data," *Seismological Research Letters*, Vol. 68, No. 1, pp. 180-189.

Schuster, R.L., R.L. Logan, and P.T. Pringle, 1992. "Prehistoric rock avalanches in the Olympic Mountains, Washington," *Science*, Vol. 258, pp. 1620-1621.

Seed, H.B., and I.M. Idriss, 1970. "Soil moduli and damping factors for dynamic response analyses," Report No. EERC 70-10, Earthquake Engineering Research Center, University of California, Berkeley, California.

Silva, W.J., 1987. "WES RASCAL code for synthesizing earthquake ground motions," *Miscellaneous Paper S-73-1, Report 24*, Waterways Experiment Station, U.S. Army Corps of Engineers, Vicksburg, Mississippi, 73 pp.

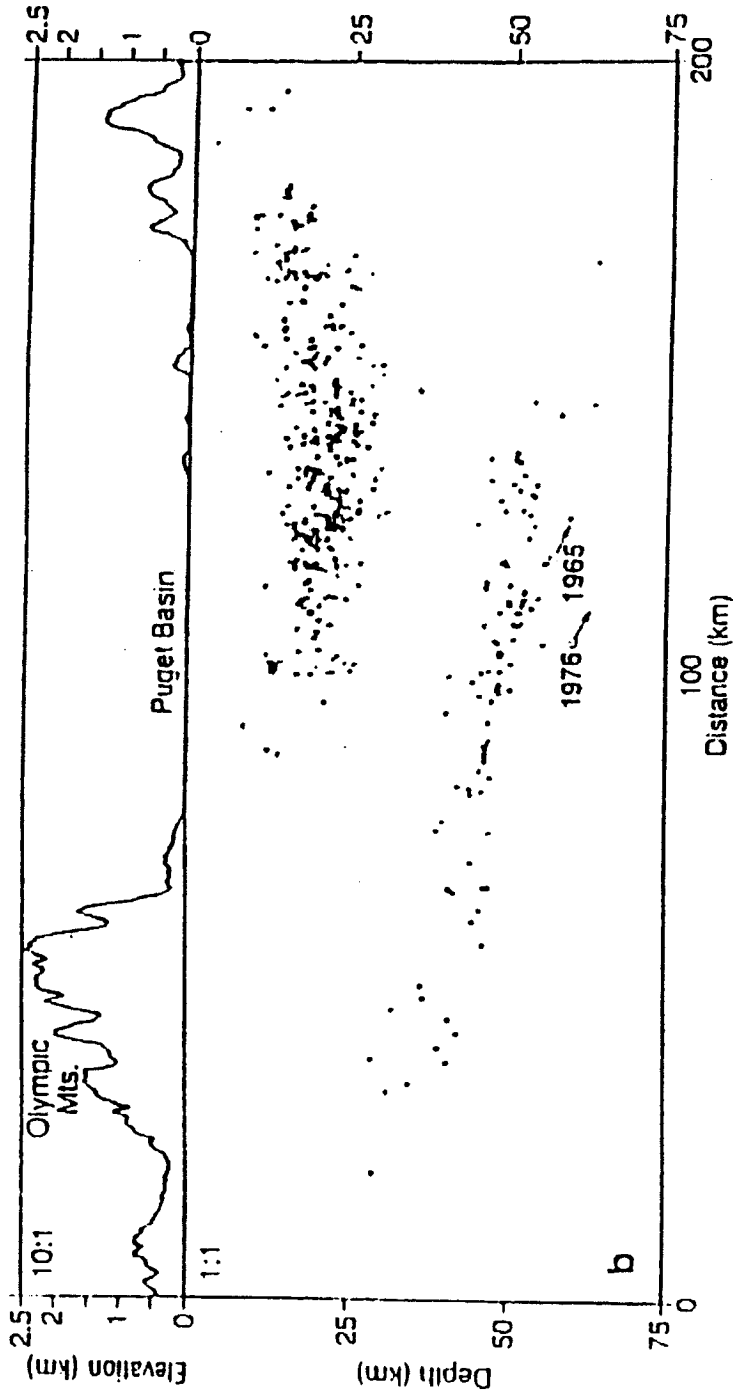
Tichelaar, B.W., and L.J. Ruff, 1993. "Depth of seismic coupling along subduction zones," *Journal of Geophysical Research*, Vol. 98, pp. 2017-2037.

Youngs, R.R., S.J. Chiou, W.J. Silva, and J.R. Humphrey, 1997. "Strong ground motion attenuation relationships for subduction zone earthquakes," *Seismological Research Letters*, Vol. 68, No. 1, pp. 58-73.

Wells, D.L. and K.J. Coppersmith, 1994. "New empirical relationships among magnitude, rupture length, rupture area, and surface displacement," *Bulletin of Seismological Society of America*, Vol. 84, pp. 974-7002.

F:\docs\jobs\497830\psha memo.doc

Typical Cross Section Through Northwest Washington State



Typical cross section through northwest Washington state showing hypocenters of earthquakes since 1970. Shallow and deep zones of seismicity are clearly apparent. After Ludwin et al. (1991).

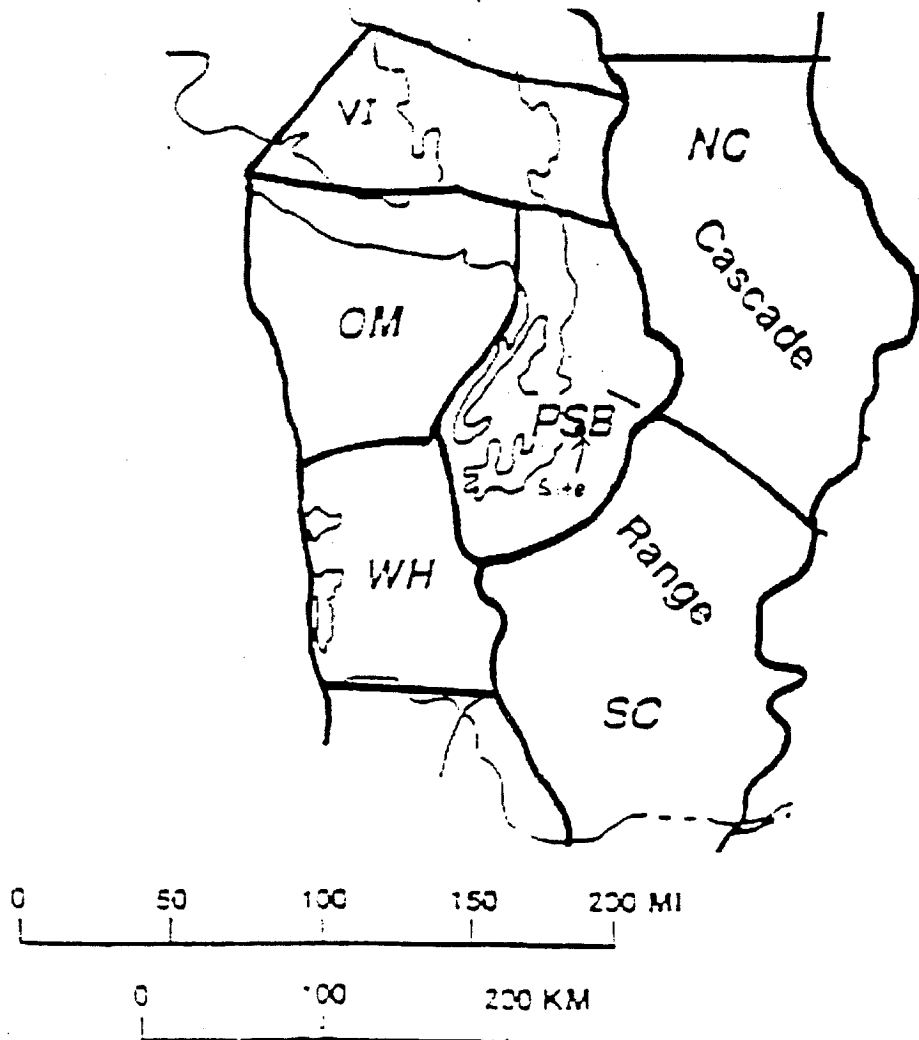
STIA 00536



J-4978-30 1/01
Figure 1

AR 049851

Shallow Seismic Source Zones Used in Recurrence Relationships



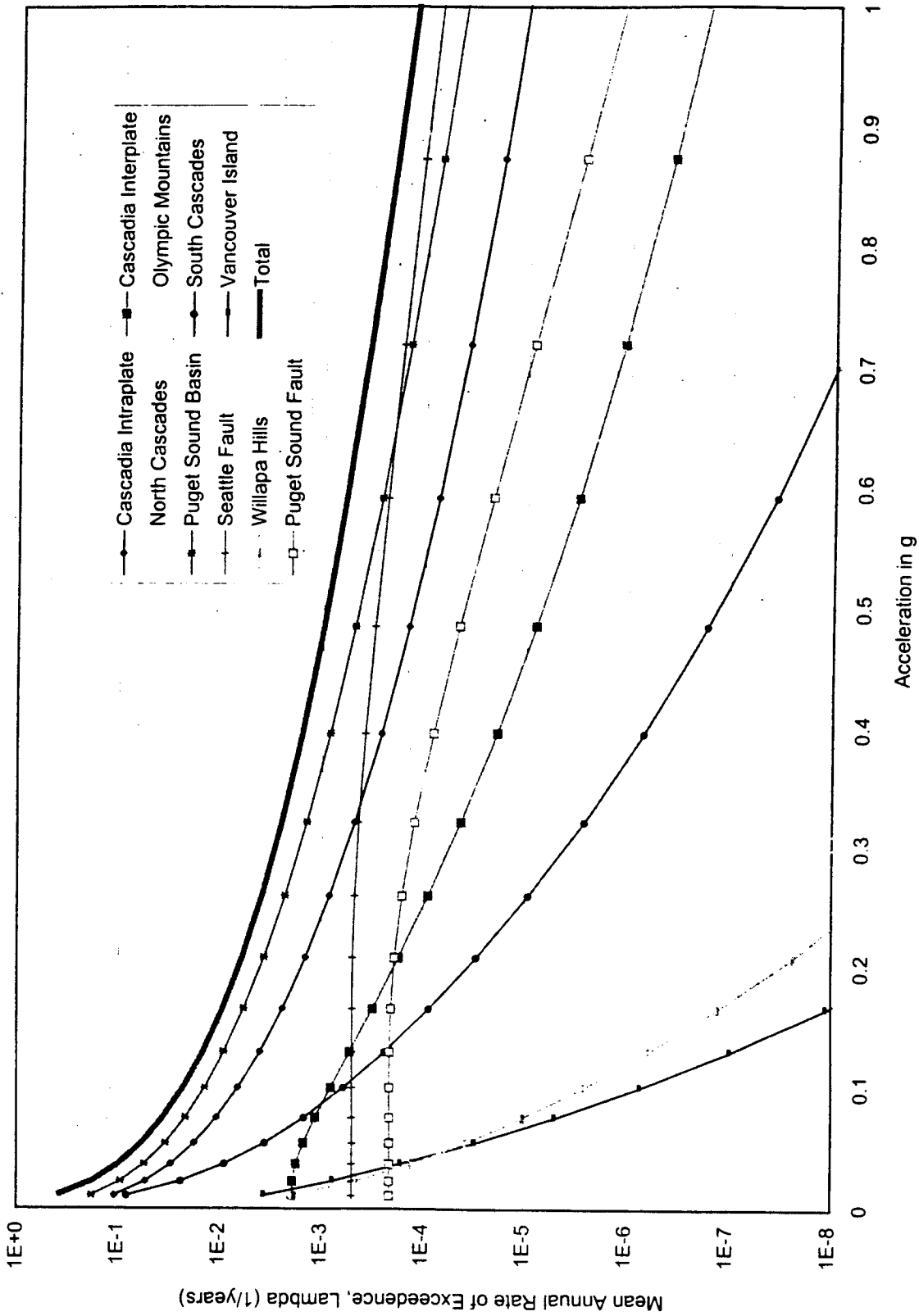
Shallow seismic source zones used to develop resources relationships for PSHA: Puget Sound Basin (PSB), Vancouver Island (VI), Olympic Mountains (OM), Willapa Hills (WH), Southern Cascades (SC), and Northern Cascades (NC).

STIA 00537


HARTCROWSER

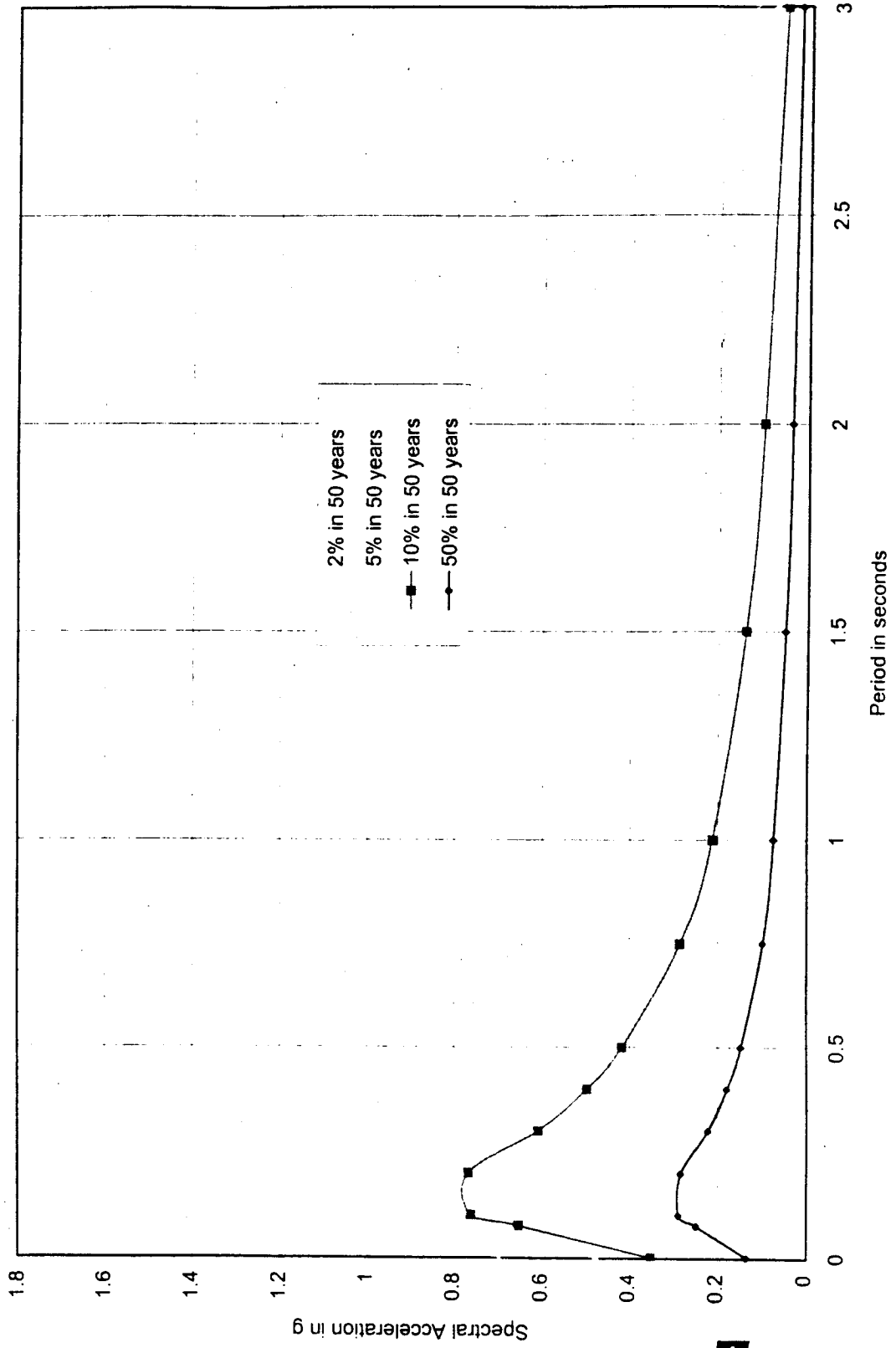
J-4978-30 1/01
Figure 2

Seismic Hazard Curves for Peak Acceleration



497830/psha figures/paul spectral accel and pha hazard.xls - Paul - Seismic Hazard for PHA

Uniform Risk Spectra



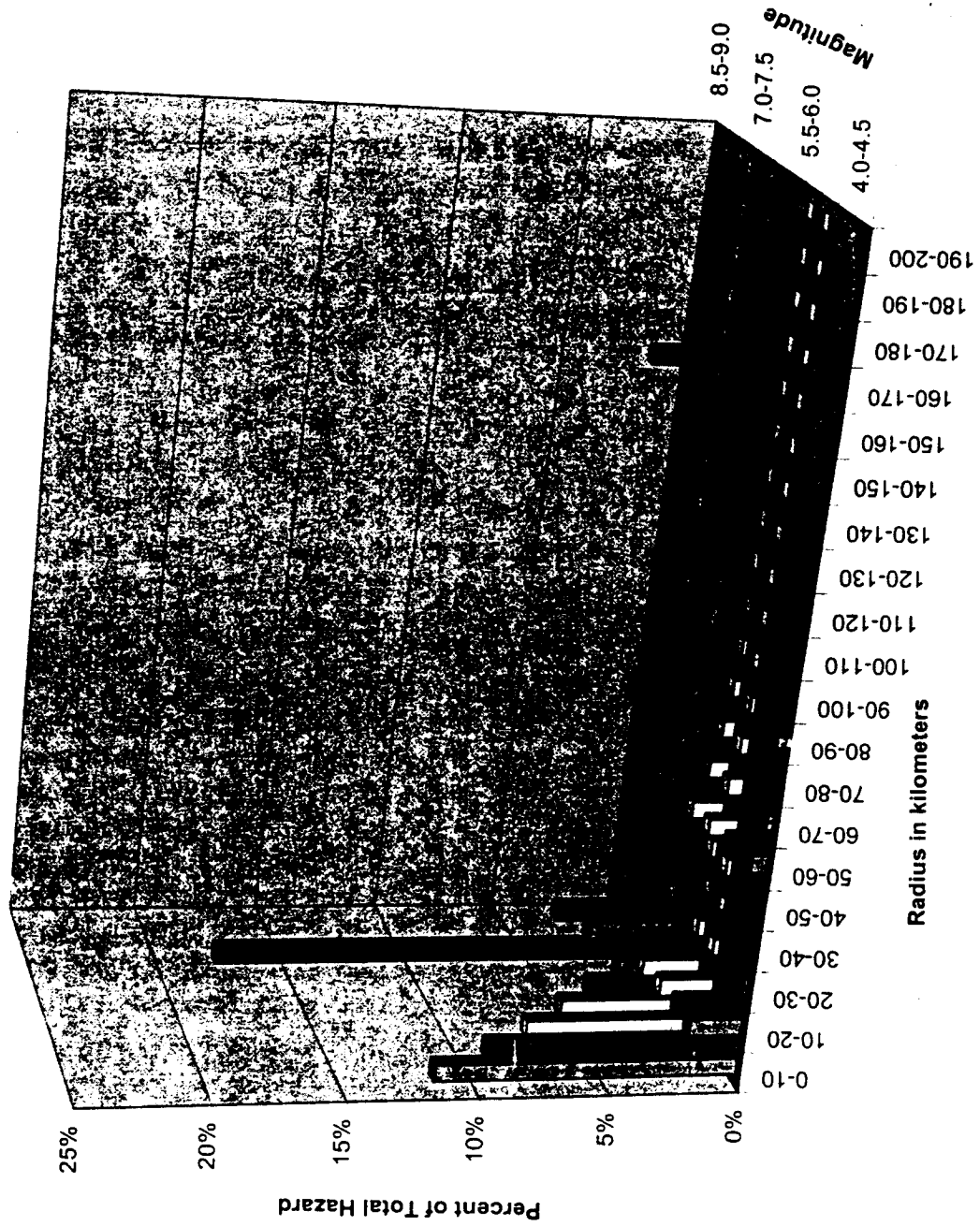
J-4978-30 1/01

Figure 4

AR 049854

STIA 00539

**Deaggregated Seismic Hazard
PHA, 475-yr seismic event**



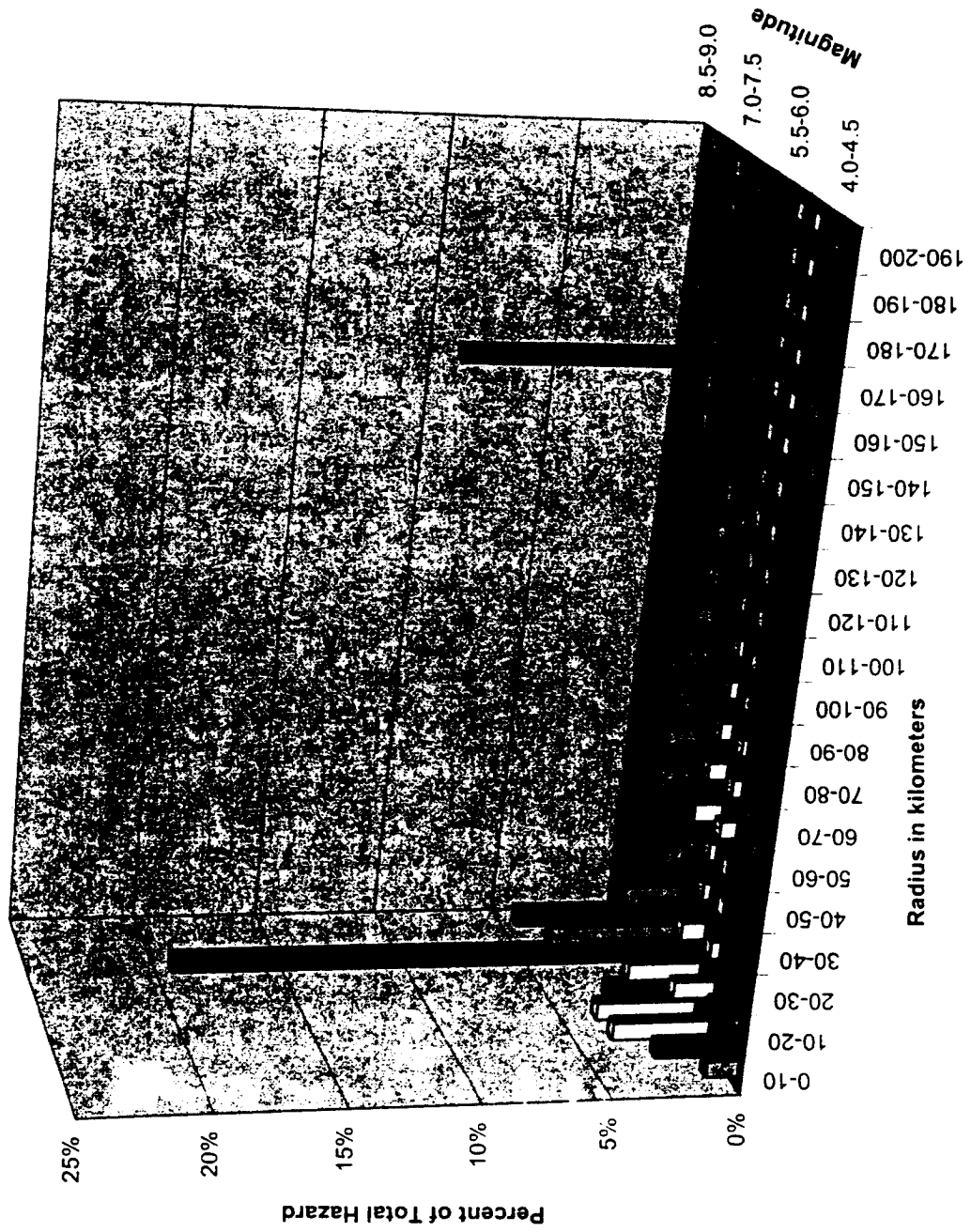
STIA 00540



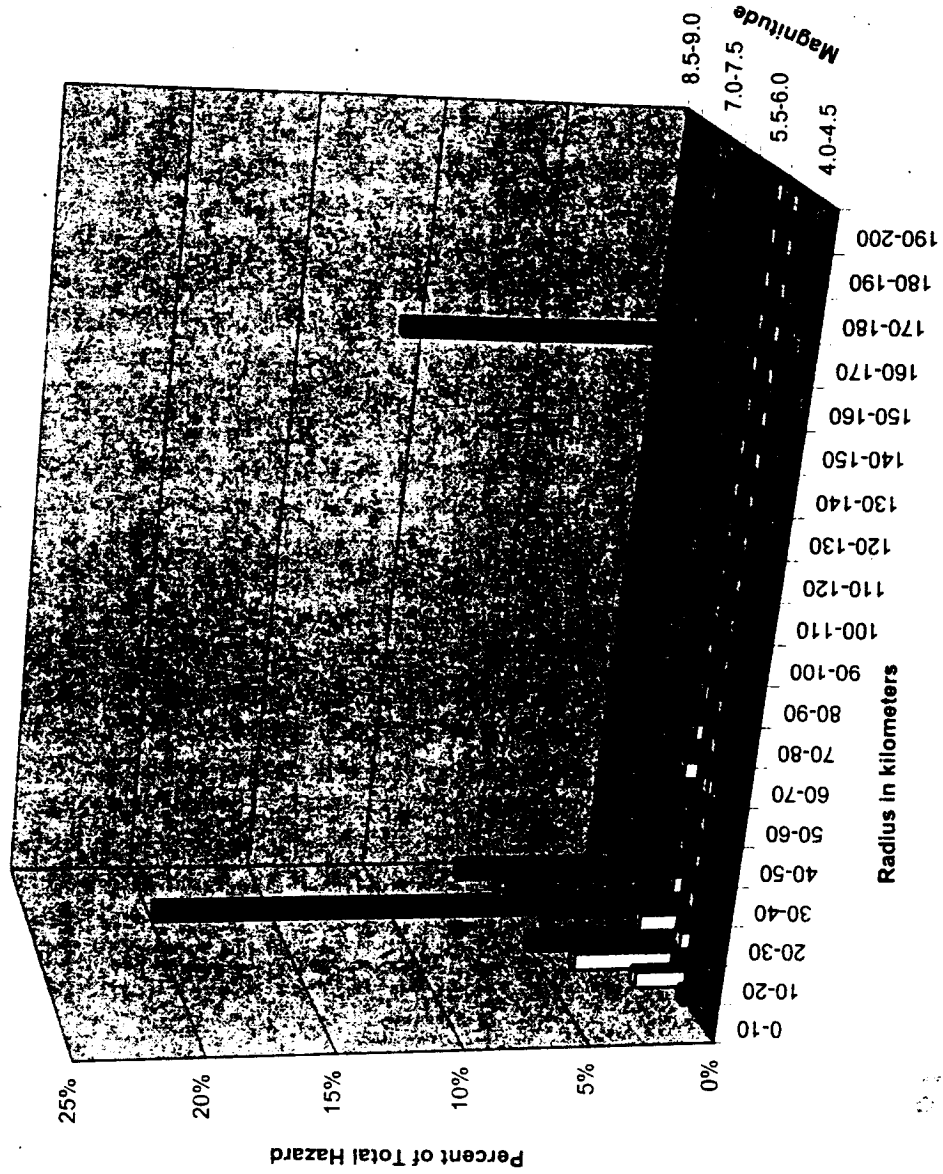
J-4978-30 1/01
Figure 5

AR 049855

**Deaggregated Seismic Hazard
T=0.5 second, 475-yr seismic event**



**Deaggregated Seismic Hazard
T=1.0 second, 475-yr event**



STIA 00542

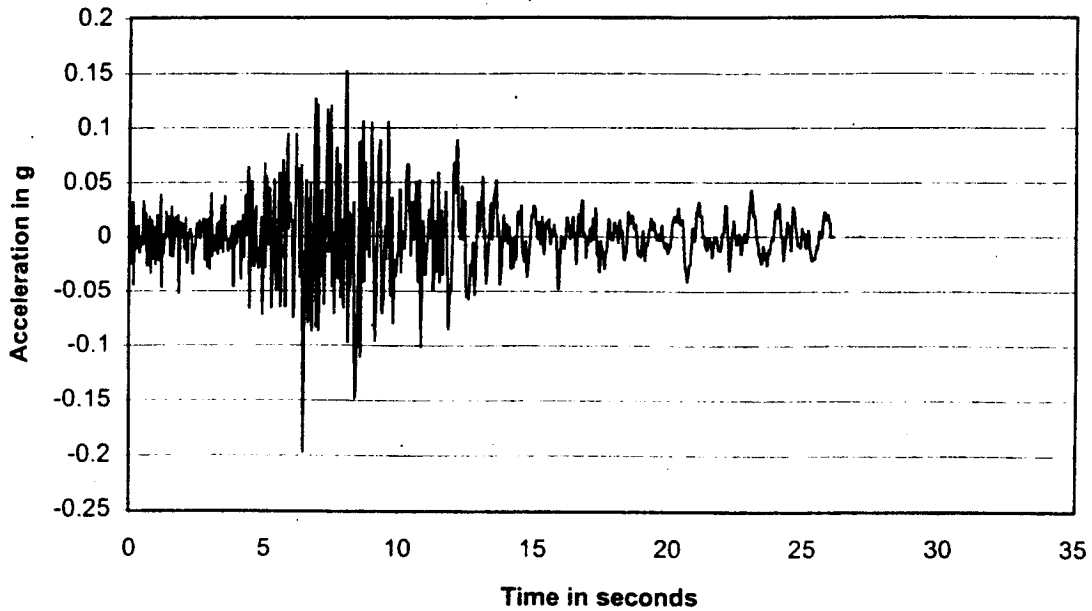


J-4978-30 1/01
Figure 7

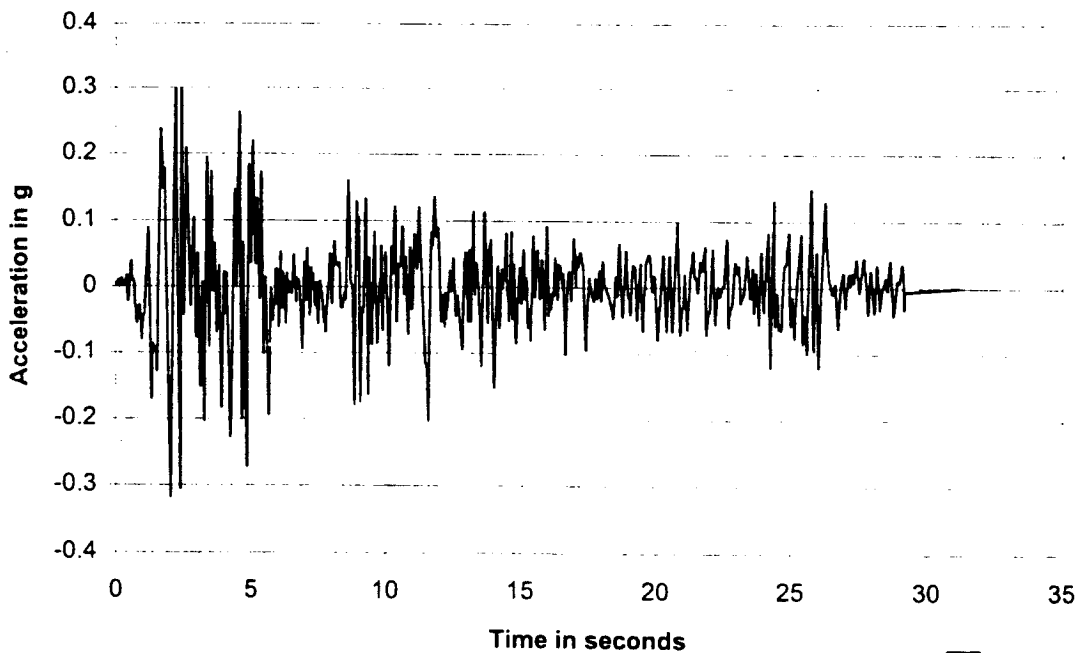
AR 049857

Time Histories of Acceleration - Seed Motions

(a) Seed Motion A - Olympia, 1965

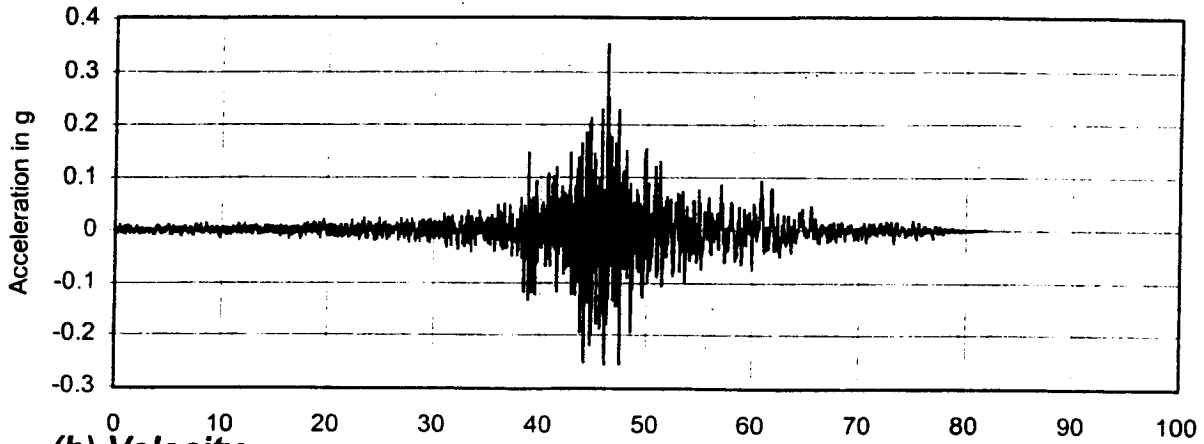


(b) Seed Motion B - El Centro, 1940

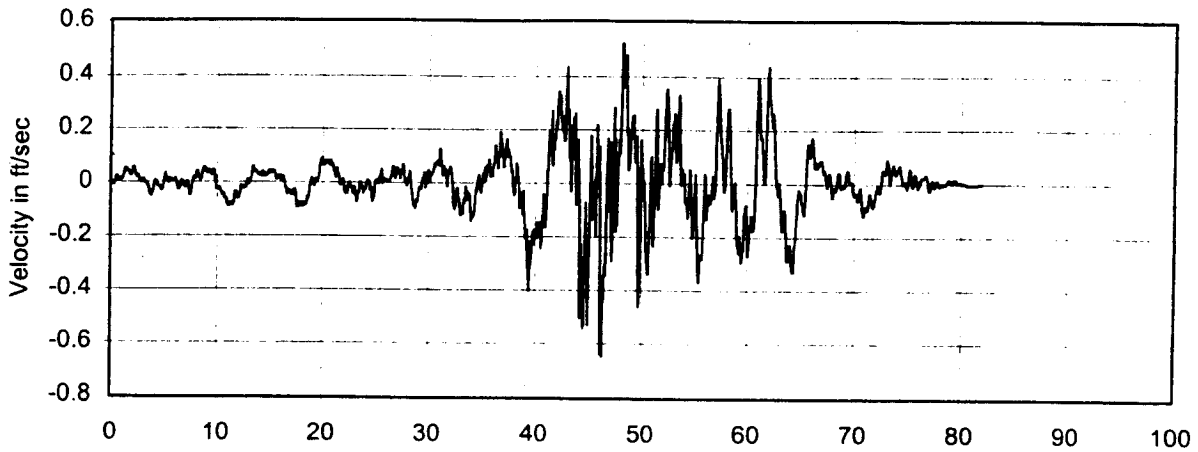


Time Histories For Motion A

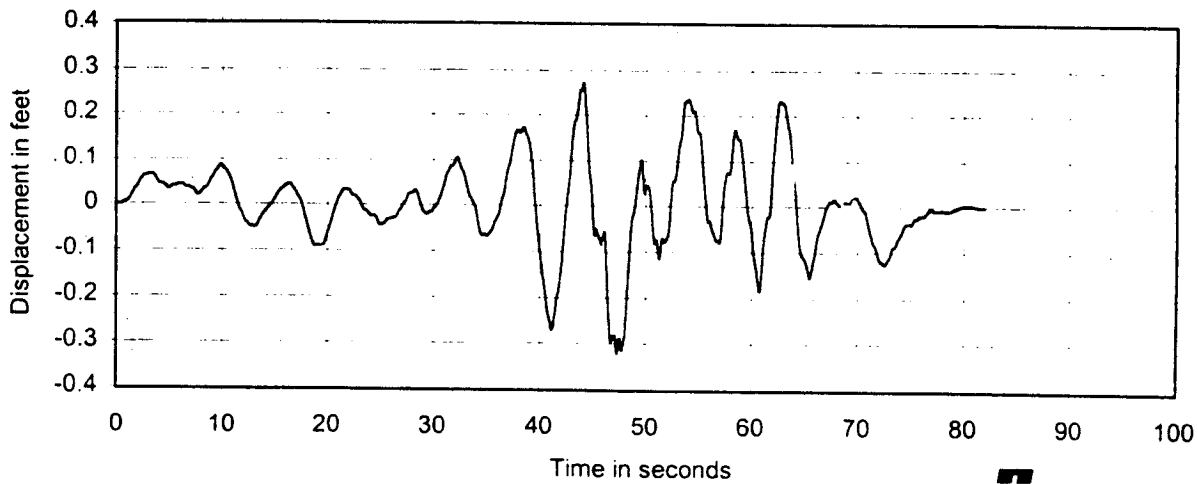
(a) Acceleration



(b) Velocity



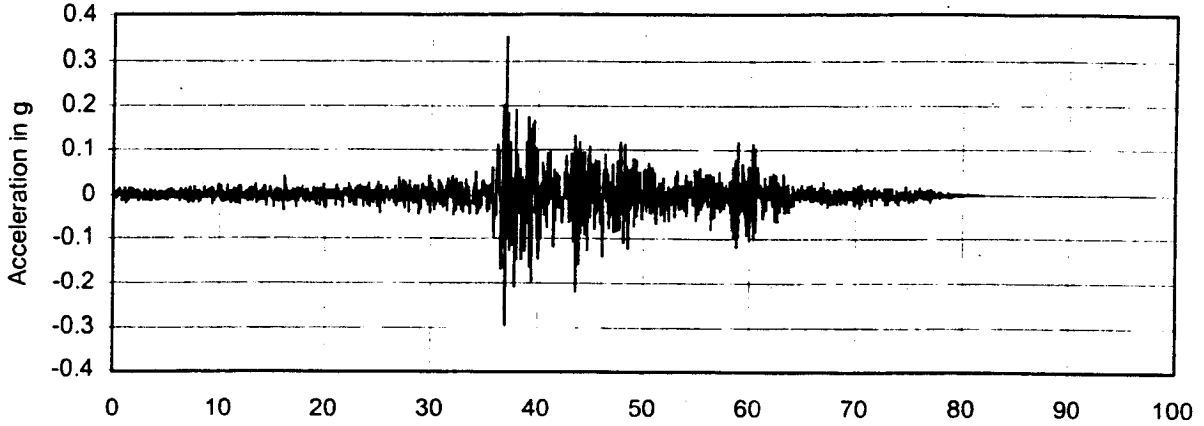
(c) Displacement



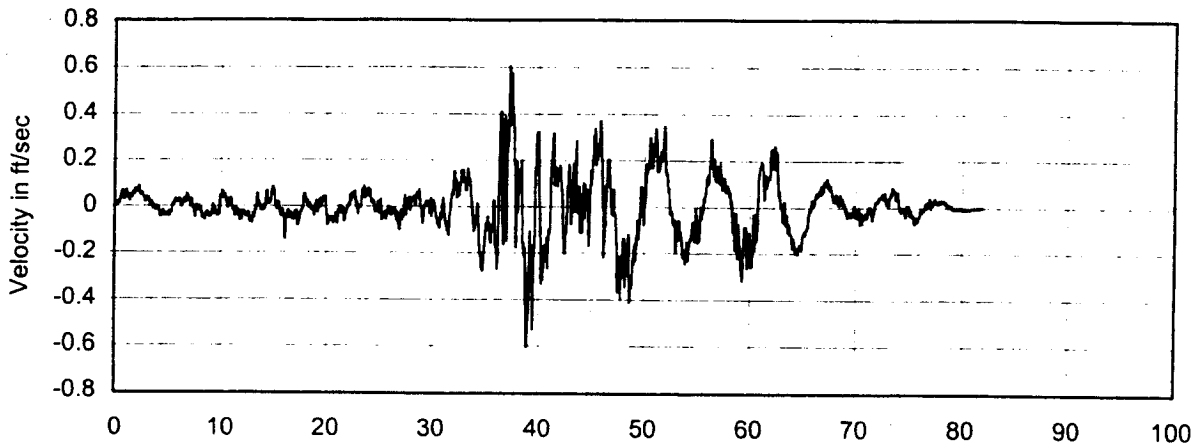
HARTCROWSER
J-4978-30 1/01

Time Histories For Motion B

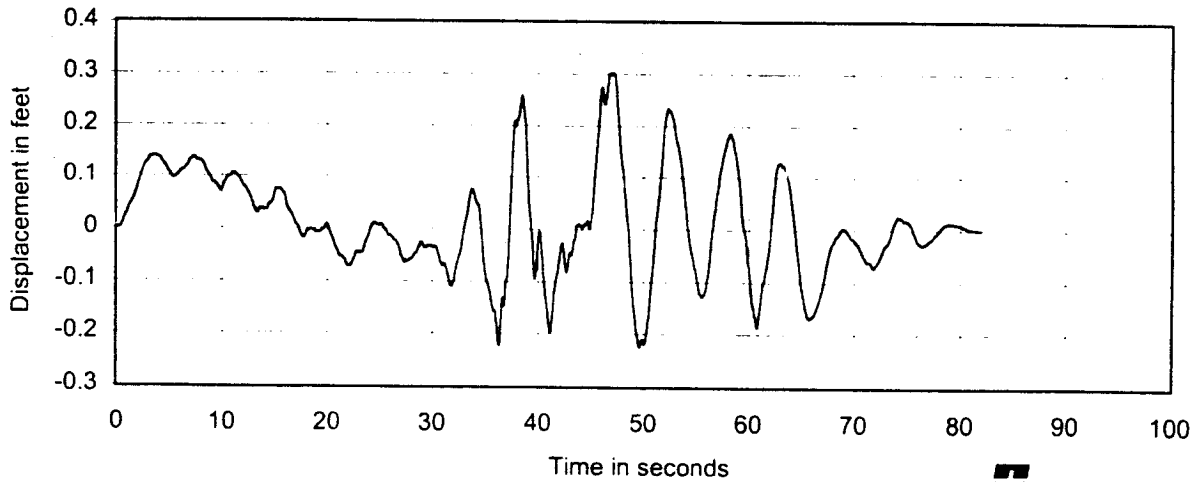
(a) Acceleration



(b) Velocity

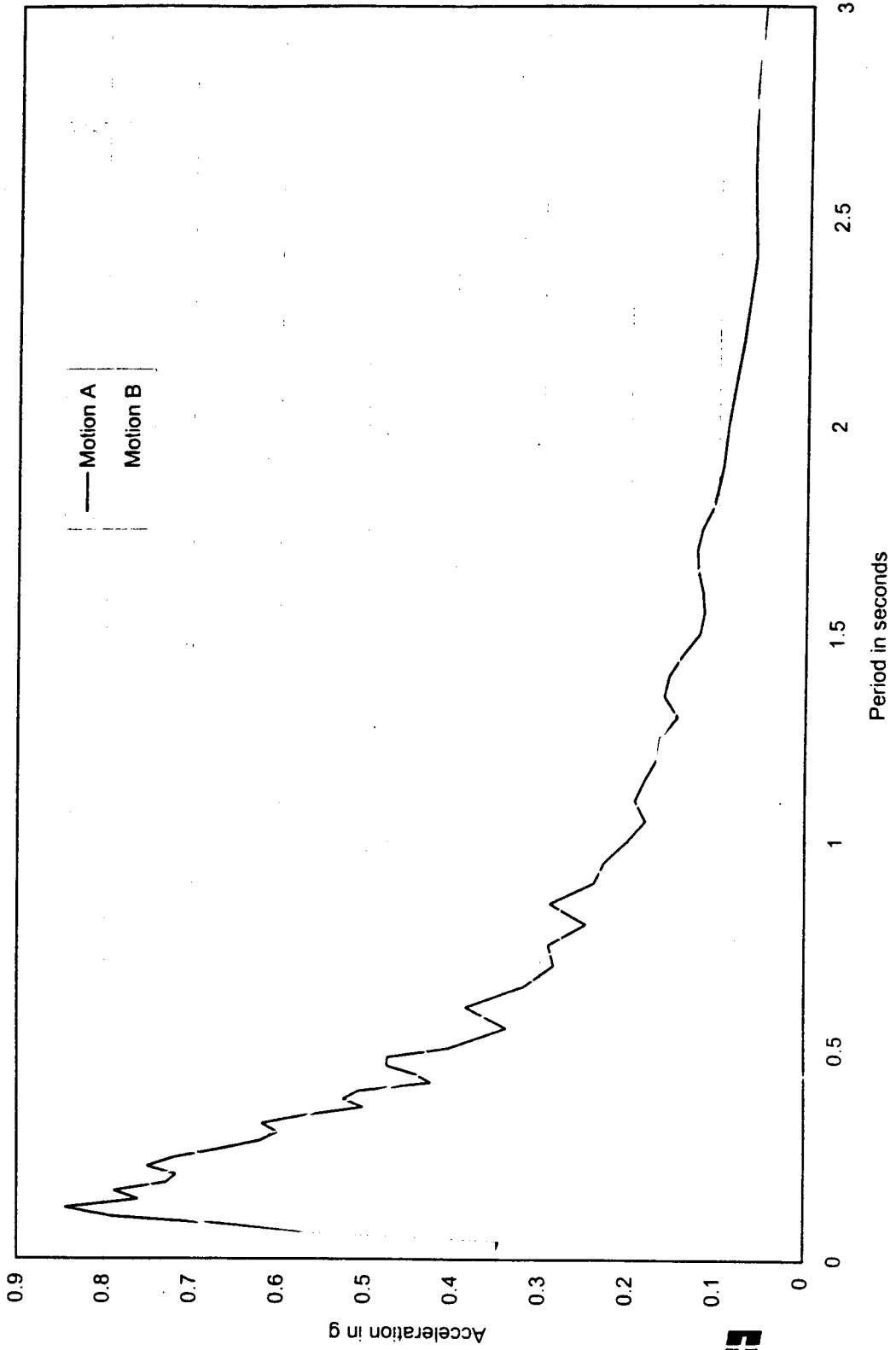



(c) Displacement



HARTCROWSER
J-4978-30 1/01

Response Spectrum 5% Damping



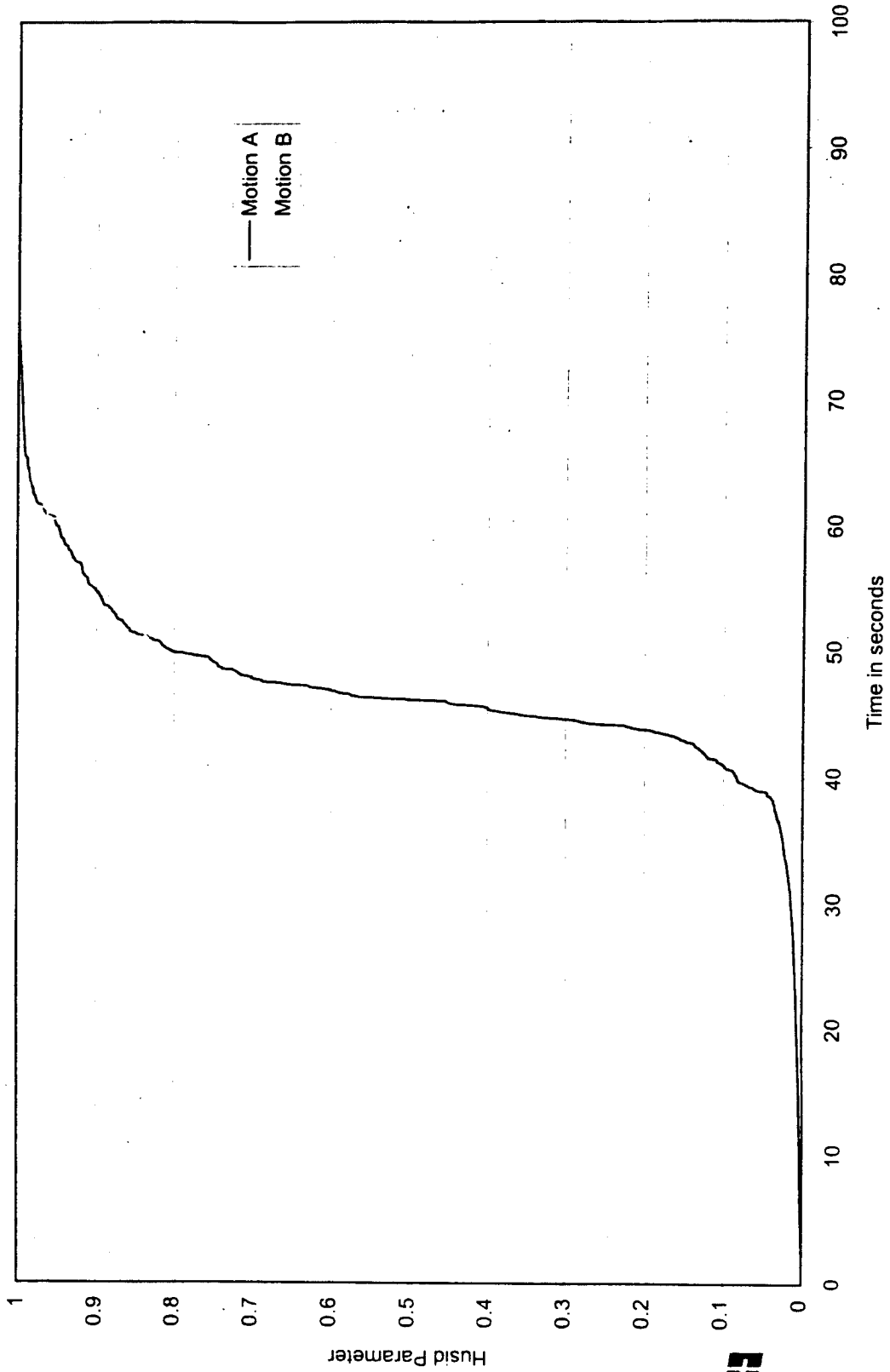

HARTCROWSER
J-4978-30 1/01
Figure 11

AR 049861

497830/psha figures/3rd Runway Embankment - Various plots_rev2.xls - Response Spectrum(rev2

STIA 00546

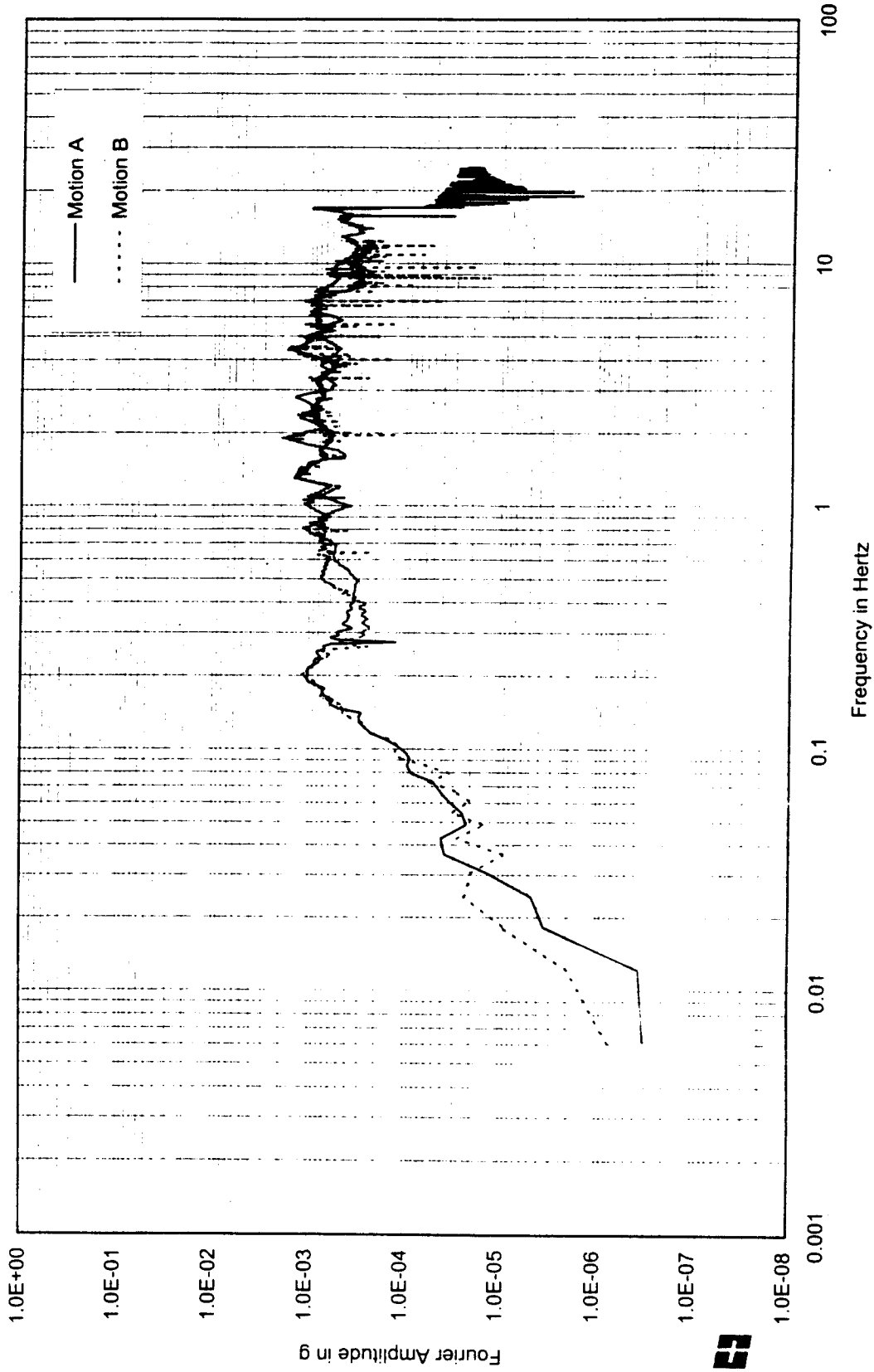
Husid Plots of Input Motions



HARTCROWSER
J-4978-30 1/01
Figure 12

AR 049862

Fourier Amplitude of Acceleration



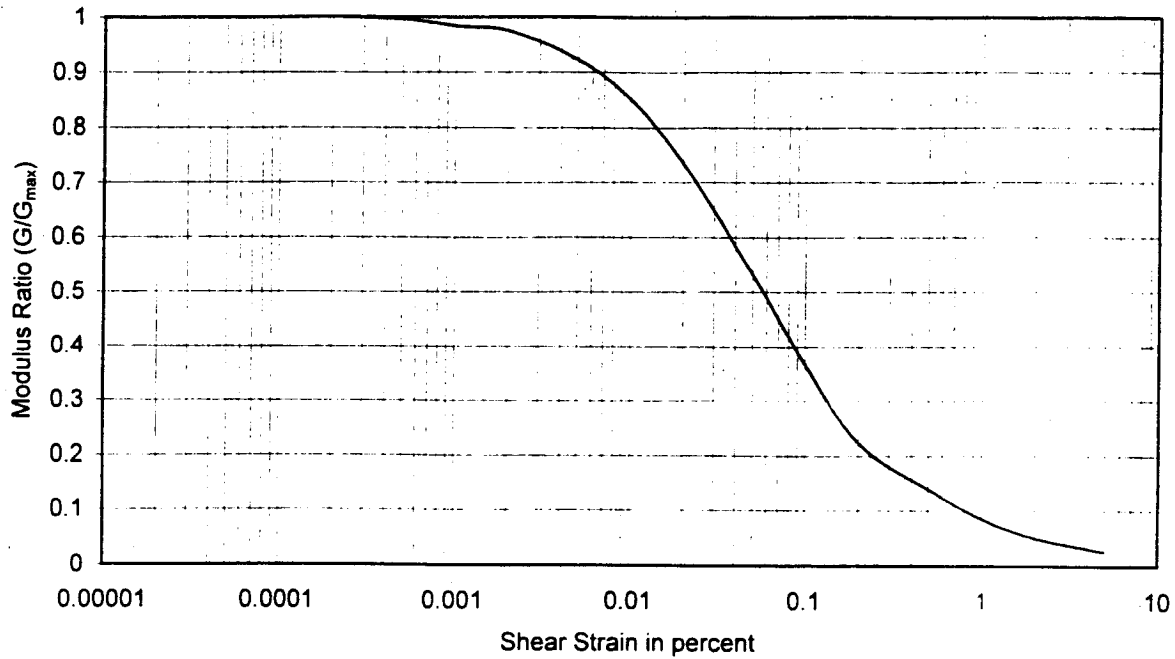
HARTCROWSER
J-4978-30 1/01
Figure 13

AR 049863

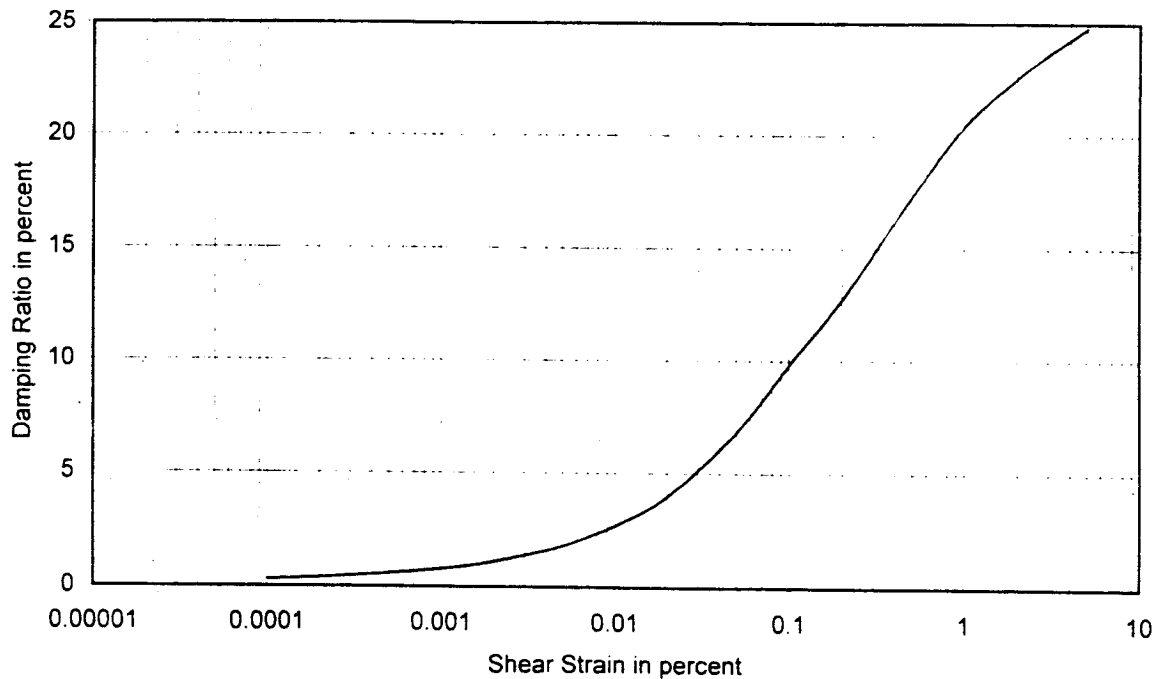
497830/psha figures/3rd Runway Embankment - Various plots_rev2.xls - Fourier Amp of Accel. (rev 2)

STIA 00548

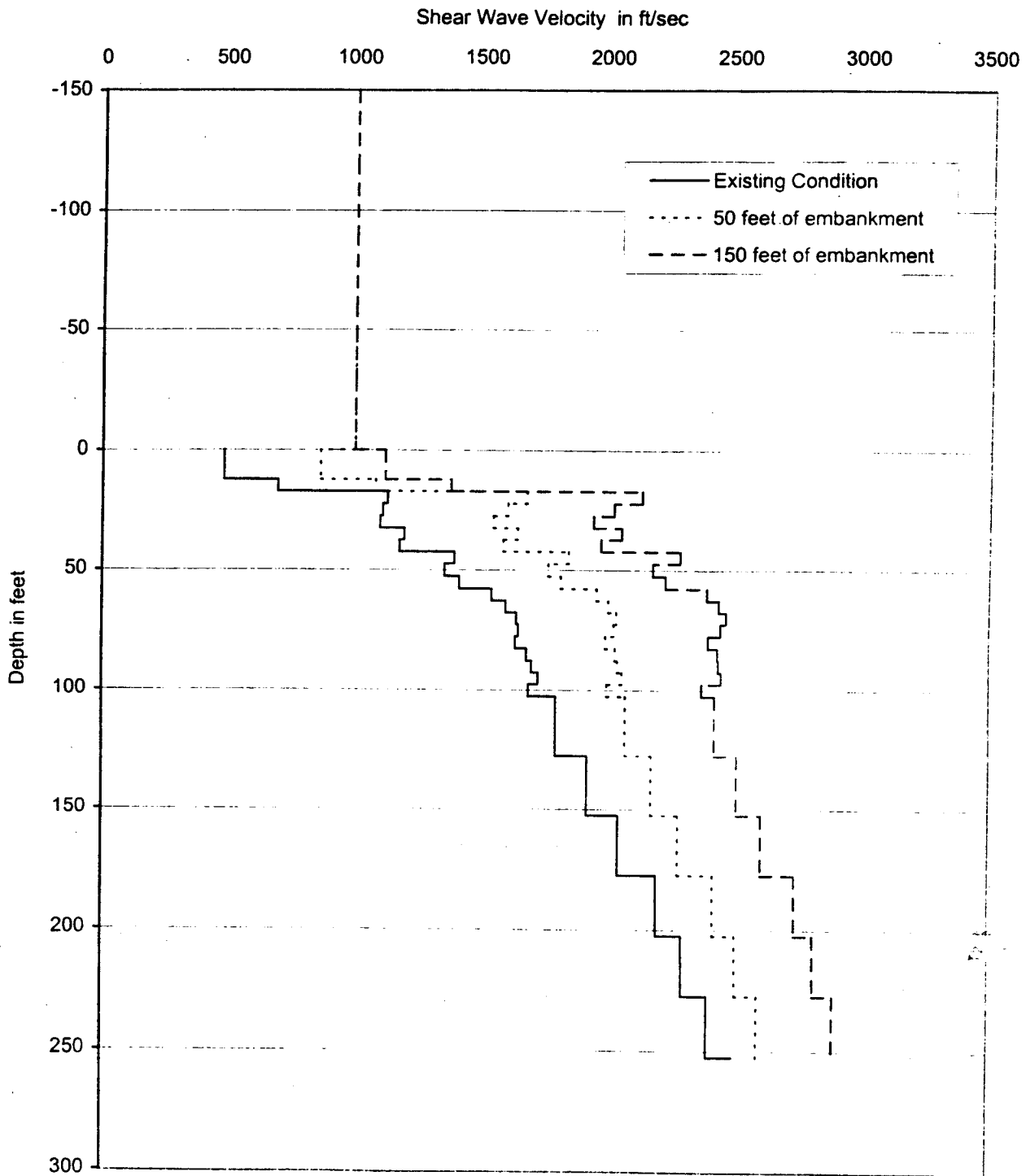
(a) Modulus Reduction Curve
Upper Bound (Seed and Idriss, 1970)



(b) Damping Curve
Lower Bound (Seed and Idriss, 1970)



Shear Wave Velocity Profiles



HARTCROWSER
 J-4978-30 1/01

497830/psha figures/3rd Runway Embankment - Various plots_rev2.xls - v_s vs depth_plot

Figure 15

STIA 00550

AR 049865